Original Article

The aerodynamic development of the new Porsche Cayenne

Thomas Wolf (iD)

Abstract

With significantly enhanced performance, the third generation of the Porsche Cayenne is even more closely oriented towards the principles of sports cars. In addition to improving the driving-dynamic characteristics, the aim of the development was to lower the drag as a contribution towards the reduction of fuel consumption and emissions. Increasing performance and a simultaneous reduction of drag are conflicting objectives, which led to a number of aerodynamic challenges during the development of the new Cayenne. In addition to detailed aerodynamic optimisations, the solution for the new Cayenne consisted of an extended adaptive aerodynamic concept, which enables a compromise between fuel consumption, performance, and comfort depending on the driving condition. The first part of the concept comprises an extended air flap system that, for the first time, enables complete closing of all cooling air inlets in the front end. The second part of the concept is reserved for the top-of-the-range V8 Turbo model and consists of a multifunctional deployable roof spoiler that adapts to the aerodynamic characteristics of the relevant driving condition and features an air-brake function as a highlight.

Introduction

The Porsche Cayenne, which was first introduced to the market in 2002, was designed as a sporty sports utility vehicle (SUV) from the outset. Outstanding performance and driving-dynamic characteristics on the road, race-track suitability, best-in-class braking performance without compromising off-road capability, day-to-day usability, and comfort have been and remain the development objectives for each Cayenne generation to this day. On the other hand, aerodynamics has become increasingly important in recent years due to environmental aspects, CO_2 legislation and the new Worldwide Harmonised Light-Duty Vehicles Test Procedure (WLTP) driving cycle.[1] Low drag is an important variable for the reduction of fuel consumption and emissions. For the new Cayenne, the specifications therefore included not only an increase in driving-dynamic performance but also a reduction in drag.

In aerodynamic terms, performance in a sporty SUV is synonymous with adequate rear-end stability, that is, a defined downforce at the rear axle and the provision of sufficiently high cooling air mass flows for engine and brake cooling in all driving situations. These objectives conflict with a reduction of drag. The associated

challenges become greater from generation to generation in view of the increasing engine power. On the current Cayenne, the first-time use of mixed tyres with larger rim dimensions and tyre widths, as well as a 44 mm increase in the vehicle width, represent an additional aerodynamic burden compared to the predecessor model.

Nevertheless, the development objective was to reduce the drag by at least 10–20 drag counts (3–5%) compared to the predecessor of the new Cayenne (Figure 1 and Table 1).

The totality of all the development tasks for the new Cayenne, including the obligatory comfort aspects, such as soiling prevention of the side windows and exterior mirrors, as well as comfort when driving with the sunroof open, led to a significant aerodynamic development effort in the case of the new Cayenne.

Flow simulations (computational fluid dynamics (CFD)) and wind tunnels were used as development

Dr. Ing. h.c. F. Porsche AG, Stuttgart, Germany

Corresponding author:
Thomas Wolf, Dr. Ing. h.c. F. Porsche AG, Entwicklung, Porschestraße 911, Weissach 71287, Germany.
Email: thomas.wolf@porsche.de

Figure 1. The new Porsche Cayenne $C_d = 0.34$.

Table 1. Performance data – Porsche Cayenne MY 2017.

Engine	V6 Turbo	V6 Biturbo	V8 Biturbo
Displacement	2995 cm^3	2894 cm^3	3996 cm^3
Engine power	340 hp	440 hp	550 hp
0–100 km/h[a]	5.9 s	4.9 s	3.9 s
Top speed	255 km/h	265 km/h	286 km/h

MY: Model Year.
[a]Sport Plus mode.

tools. The aerodynamic simluations were performed with PowerFLOW.[2] This software is based on the Lattice–Boltzmann equations[3,4] and is well known in the automotive industry.[5–8] The code simulates discrete fluid particles and enables inherently transient simulations on a Cartesian, structured grid. Very large eddy simulation (VLES) was used for turbulence modelling and the sliding mesh technique[6] to simulate transient rotation of the wheel rim and spokes. The work of Kotapati et al.[2] provides a good review of the Lattice–Boltzmann simulation approach using the VLES turbulence model and describes the capabilities for aerodynamics, and thermal and aero-acoustics applications for production vehicle development.

The main wind tunnel used for the development of the Cayenne was the new Porsche full-scale aerodynamic and aeroacoustic wind tunnel (NWT).[9] The tunnel which went into operation in 2015 achieves a

top wind speed of 300 km/h and is equipped with state-of-the-art ground simulation techniques for series and race car development. Furthermore, during tunnel calibration, the flow field in the test section was adapted to the flow field on the road with the aid of full-scale reference vehicles.[10] The unique key feature of the tunnel is the interchangeable belt system. This comprises a five-belt configuration for series car development and a single wide-belt configuration which is mainly used in race car development weighing more than 20 tonnes each. Both systems can be exchanged within 3 h which offers a great flexibility for series and race car development.

However, because the new full-scale wind tunnel was only ready in 2015, different external wind tunnels with five-belt ground simulation were used during the 2012–2014 period. As a result of the development, the C_d value for the new Cayenne was reduced by 20 drag counts to $C_d = 0.34$ compared to the predecessor.

The development process and the methodology for the aerodynamic development of the new Cayenne will be described briefly below. The individual aerodynamic optimisations will then be described in detail with an emphasis on the adaptive aerodynamics, that is, the active air flap system and the adaptive roof spoiler of the Cayenne Turbo. Finally, the aerodynamic properties of the new Cayenne will be summarised and compared with the predecessor vehicle.

Development process

The aerodynamic development process is integrated in the product and vehicle development process. It consists of the product definition, concept development and validation, production development, and finally the production preparation and start phases (Figure 2). Before the actual project start, there is a several month-long preliminary phase in which activities relating to overarching topics such as modules and platforms are held, the vehicle concept is elaborated and the vehicle target values are defined, which are documented in the so-called vehicle profile.

This early pre-project phase has become increasingly important in recent years because in the context
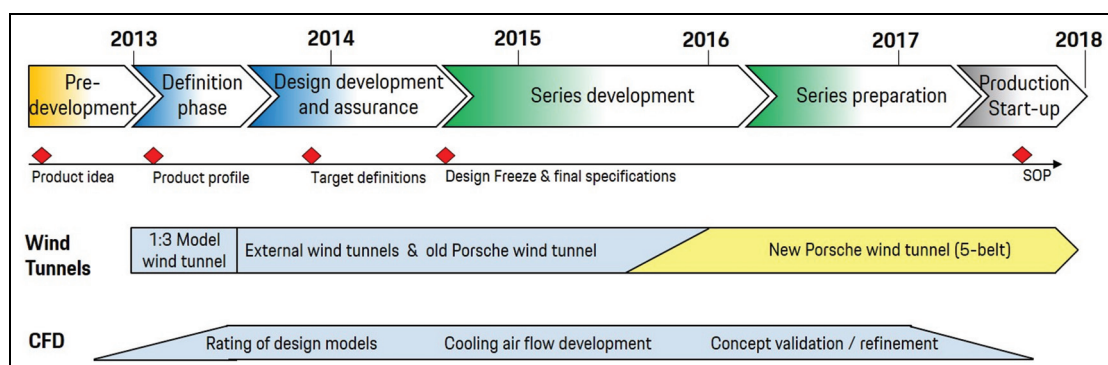

Figure 2. Development process and tools used.

of 'overall vehicle target value definition', the aerodynamic target values are already defined and filed by the aerodynamics engineers together with stylistic and engineering measures as well as a specifications catalogue. Approximately 80% of the aerodynamic concept is elaborated and defined during this phase.[11]

One of the important phases for the aerodynamic development is the first project phase, the so-called product definition. In this phase, several 1:1-scale proportional models and up to four 1:3-scale styling models are built by the design department for aerodynamic evaluation. With the new Cayenne, both the proportional models and styling models were evaluated experimentally at the Porsche 1:1 and 1:3 wind tunnels and by means of flow simulations. A 1:3 model of the predecessor vehicle was used as a reference. Simultaneously, in-house proportion and aerodynamic studies were conducted on 1:3 clay models at the model wind tunnel. The tunnel used is a reduced scale model of the old full-scale wind tunnel (OWT).[12–14] It was upgraded with distributed boundary layer suction and a five-belt ground simulation system in 1998.[15] A few years later, it was upgraded from the original 1:4 scale to 1:3 scale and has been intensively used for model scale testing in the last 20 years.

At this point, it should be mentioned that model wind tunnel testing has its limitations, especially when it comes to the correlation of absolute force coefficients to full-scale wind tunnel or CFD results. The reasons for this are the limited geometric fidelity of the scale models, the reduced Reynolds number and often also the absence of representative cooling air flows.[16] Nevertheless, the in-house experiences in the past have shown that trends and increments are well covered and consistent to the trends and results from the full-scale wind tunnels which is in line with the recent study of Meinert et al.[17] Thus, the model wind tunnel is a very efficient tool for proportional and design studies because numerous proportion and styling variants can be examined in a short time, which is currently not possible within a comparable timeframe using CFD simulations.

During the second project phase, the concept development phase, the main focus was on evaluating and supporting the two selected design form themes aerodynamically until selection of the final design. At the same time, the first 1:1-scale aerodynamic test object, the so-called throughflow body (TFB) and CFD models for various engine versions were built. The TFB represents the so-called development vehicle with a defined engine version. The initial construction of the TFB consisted of a clay structure, including engine and radiators. The radiators are equipped with pressure-metering equipment for measuring cooling air volume flows and were previously calibrated on an airflow test stand. For the measuring principle and methodology, see literature.[18–20] The counterpart of the TFB on the simulation side is the VTFB, the virtual TFB. On the current Cayenne, CFD was principally used to cover the cooling air mass flows for the individual engine versions, Figure 3.
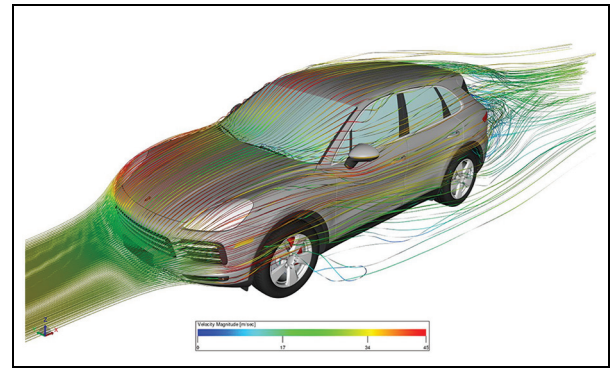
Figure 3. CFD simulation of external and internal flow.

**Figure 4.** Full-scale wind tunnel model ('Aerobuck').

Following the design freeze, the 1:1 TFB clay model was replaced with a partially modular 1:1 TFB model with a glass fibre-reinforced plastic (GFRP) outer skin built onto an Audi Q7 chassis (PL73). During the remaining development period, the model (Figure 4) was used intensively for detail optimisation of the flap systems, add-on parts and underbody panelling, as well as for investigating and optimising exterior mirror and side window soiling prevention.

The development of the new Cayenne took place during the period from late 2012 to mid 2017. The great challenge here was that the new full-scale in-house wind tunnel with a modern ground simulation only became available from mid 2015. Although a number of aerodynamic tasks could still be carried out very well in the old full-scale wind tunnel without ground simulation, measurements in a wind tunnel with modern ground simulation are imperative for optimisation and fine-tuning of aerodynamic measures and in particular for the adjustment of the desired lift forces at the front and rear axle. For this reason, significant time had to be booked at external 1:1 wind tunnels with suitable ground simulation and a significant part of the aerodynamic developments carried out there at the beginning of the development activities. In addition to the in-house 1:3 model wind tunnel, a total of four full-scale aerodynamics wind tunnels

Table 2. Breakdown of 1:1 wind tunnel hours.

Wind tunnel	Ground simulation	Share
Porsche OWT	Fixed ground	38%
S2A	5-belt	8%
FKFS	5-belt	9%
Porsche NWT	5-belt	45%
	Total:	1,051 h

OWT: old Porsche full-scale wind tunnel; FKFS: *Forschungsinstitut für Kraftfahrwesen und Fahrzeugmotoren*, University of Stuttgart, Germany; S2A: *Soufflerie Aérodynamique et Acoustique*; NWT: new Porsche full-scale Wind Tunnel.
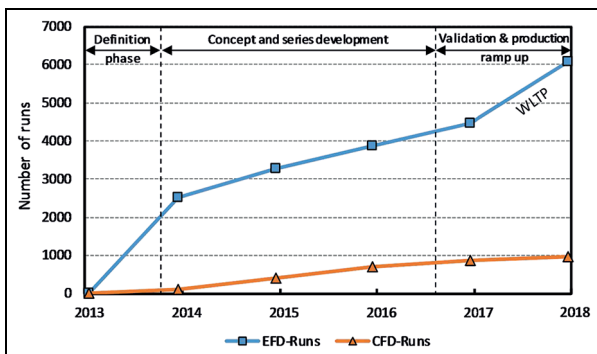
Figure 5. EFD/CFD runs during the development period.

were used for the aerodynamic development of the new Cayenne: the OWT, the *Forschungsinstitut für Kraftfahrwesen und Fahrzeugmotoren*, University of Stuttgart, Germany (FKFS) aerodynamic wind tunnel,[21–23] the *Groupement d'Intérêt Economique*, France (GIE) S2A aero-acoustic wind tunnel,[24] and from

August 2015, the NWT. Counting the FKFS thermal wind tunnel,[25] which was booked for evaluation and optimisation of the exterior mirror and side window soiling, a total of six wind tunnels have been used for the development of the new Cayenne.

By the end of 2017, a total of 1288 wind tunnel hours had been used, of which 237 h were in the 1:3 model wind tunnel and 1051 h in the 1:1 wind tunnels. Table 2 shows a break-down of the hours used at the individual wind tunnels.

Figure 5 shows a comparison of the number of wind tunnel measurements (experimental fluid dynamics (EFD) runs) conducted during the course of the development process with the number of CFD runs completed. The total number of EFD runs was 6067 and the number of CFD runs 973.

Aerodynamic optimisations

The aerodynamic optimisations of the new Cayenne can roughly be distinguished into basic shape and engineering topics, with a clear emphasis on the latter. Figure 6 gives an overview of the optimisation measures for the new Cayenne. The initial starting point for the aerodynamic optimisation of a vehicle is always the basic shape (proportions) of the vehicle. Here, there were only limited optimisation opportunities with regard to the new Cayenne because the vehicle and dimensioning concept was not intended to differ fundamentally from the predecessor. In the early project phase, a proportion study on a 1:3 clay model was conducted in the model wind tunnel, which delivered valuable information for further detailed optimisation.[26] Optimisations were implemented in the areas of
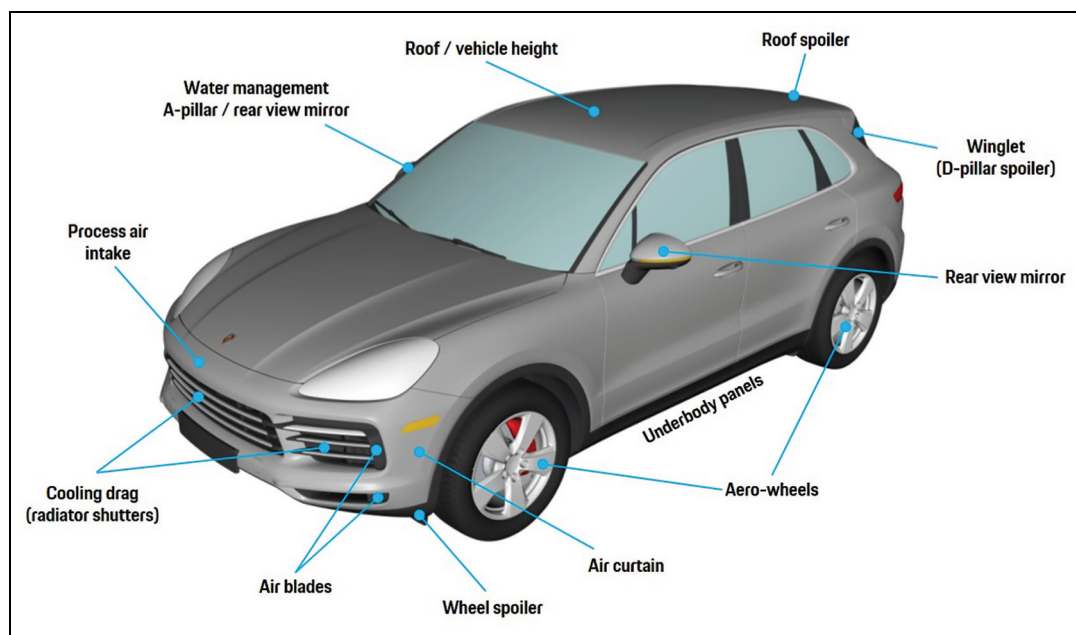
Figure 6. Aerodynamic measures for the new Cayenne.
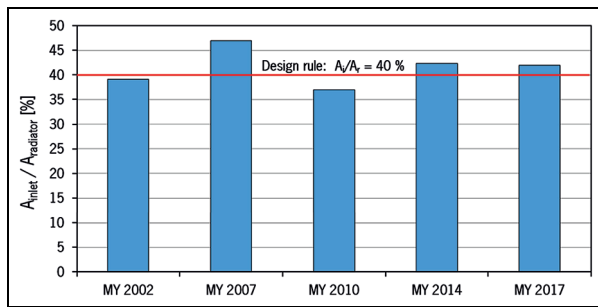
Figure 7. Relative air inlet areas of the various Cayenne generations based on the example of the Turbo.
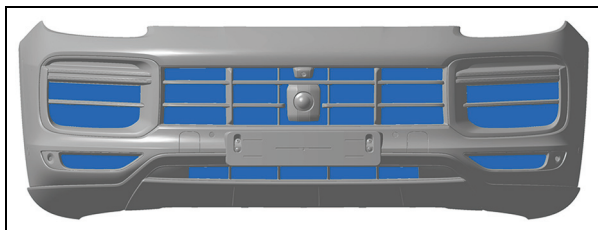
Figure 8. Net inlet areas, V8 Turbo front-end MY 2017.

windshield angle, design of the A-pillar and particularly in the roofline and roof spoiler. The roofline was lowered by 9 mm compared to the predecessor in order to at least partially compensate for the increase in vehicle cross-section resulting from the greater vehicle width.

Cooling apertures

A very important topic in the definition phase is the specification of the necessary cooling air inlet cross sections in the front end.[11,18] With the current Cayenne, no specifications for cooling air mass flows were available in terms of thermodynamics during this early project phase. The inlet sizes were therefore estimated based on the experiences with the predecessor vehicle. For the estimate, it can be assumed that the cooling air mass flows and inlet cross-sections increase roughly in proportion with the engine power.

If no predecessor vehicle is available, the '40%-rule' can be used as an estimate if the radiator size is known.[18] Using this empirically derived rule, the necessary projected net air inlet cross section can be conservatively approximated at about 40% of the radiator face area. As can be seen from Figure 7, the air inlet cross-sections on the Cayenne are roughly that size. Figure 8 shows the final state of the Turbo front end.

Air flap systems/radiator shutters

The primary approach adopted in the front section was to reduce the so-called 'cooling drag' which is the increment in drag due to the engine cooling airflows.[27] The drag increase results from the pressure losses of the
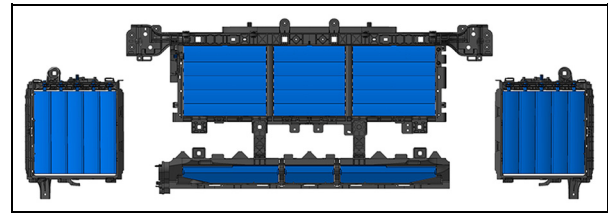
Figure 9. Air flap systems, cut out.

underhood air flow through air ductings and radiators together with momentum losses at the in- and outlets in combination with interference effects of the exiting air with the surrounding flow.[28,29] With current front engine vehicles, the cooling drag can amount to up to 10% of the total vehicle drag[30,31] where it can be assumed that the cooling drag varies linearly with the size of the inlet opening area,[32,33] that is, it increases proportionally to the cooling air mass flow rate. Thus, the reduction of cooling drag was one of the greatest individual factors for reducing the overall drag of the new Cayenne, particularly as the required cooling air mass flows for engine cooling are significantly higher compared to the predecessor. Moreover, all the new Cayenne models are equipped with turbo-charged engines. The charge air coolers are located on the sides under the front fenders and require two additional air inlets in the front end. The cooling air mass flows required for the charge air coolers result in a further increase in cooling drag. The objective from the outset was therefore demand-based control of all cooling air mass flows, that is, equipment of all air routes with controllable radiator shutters or air flap systems.

The various air inlets of the front end can be depicted from Figure 8. In addition to the upper air inlet at the centre of the vehicle, a further air inlet is located below the bumper cross member. Both inlets supply the AC condenser and the coolant radiator with cooling air. The charge air coolers positioned at the sides are also supplied with cooling air via a larger upper and a smaller lower air inlet. Figure 9 shows an overview of the assigned air flap systems. Four flap systems are used in total. A radiator shutter with five horizontal flaps is used in the central upper air inlet. The lower air inlet is controlled by a single flap. In the two side inlets, a radiator shutter with five vertically arranged flaps is used. The two central and two outer flap systems are actuated simultaneously and independently from one another. Figures 10 and 11 show an Y-section through the central flap systems and a Z-section through the left outer flap system.

The vertical arrangement of the side charge air flaps has the advantage that the maximum cooling air mass flow through the charge coolers is already available at significantly smaller opening angles than with a horizontal arrangement of the flaps. The cause for this is that the side cooling air inlets are supplied with air at an angle of approximately 35°–40° to the direction of
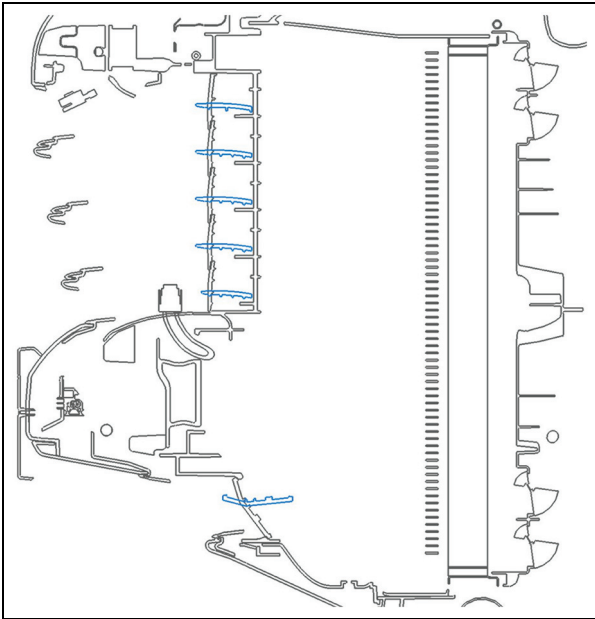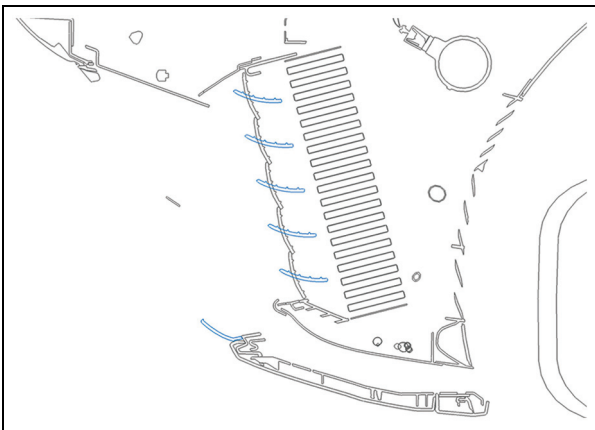
Figure 10. Centre flap systems, y-section, side view.
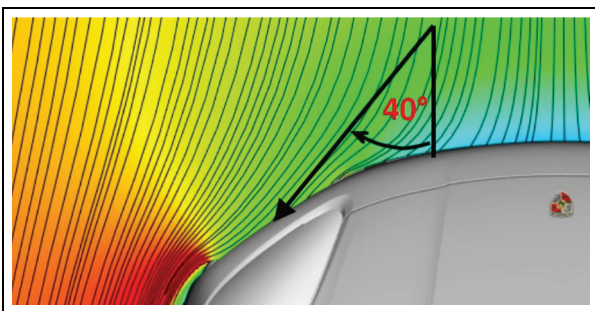

Figure 11. Side flap system,[34] z-section, plan view.

Figure 12. Lateral airflow side inlets, CFD, top view.

Figure 13. Centre/side radiator shutter characteristic.

Table 3. Influence of flap systems on the aerodynamic coefficients during full closure.

Parameter	Centre flaps	Side flaps	Total
Drag ΔC_d	−0.015	−0.007	−0.022
Front lift $\Delta C_{l,f}$	−0.04	−0.02	−0.06
Rear lift $\Delta C_{l,r}$	0.01	0.01	0.02

centre of vehicle, where the flaps are arranged horizontally. The variation of the cooling air mass flow rate with the rotation angle of the cooling air flaps is shown. As can be seen, the maximum cooling air throughput of the centre flap system is only achieved at a flap rotation angle of 90° (100% open), which corresponds to expectation. In contrast, 99.7% of the maximum cooling mass flow is already achieved at a rotation angle of only 44° in the case of the side cooling air flaps. This enables a very short response time in the case of cooling and power demands from the engine.

In the closed state, the flap systems on the new Cayenne reduce the drag by a total of $\Delta C_d = -0.022$ or 6%. Table 3 provides an overview of the influence of the individual flap systems and full closure on the aerodynamic coefficients.

The change in front-axle lift does not play a significant role in terms of driving dynamics in the case of front-engine vehicles. Changes in the rear-axle lift are relevant and were taken into account during design of the vehicle with respect to the roof spoiler.

Air blades

As with the predecessor, air blades were implemented at the outer edges of the side air inlets for the charge air coolers, see Figures 6 and 14. These air guide vanes, for which a patent application has been filed,[35] increase

travel (Figures 12 and 15), so that the flaps are already fully wind-facing at an opening angle of approximately 40°–45°.

Figure 13 presents a comparison of the characteristic of the side charge air flaps with the flap system at the
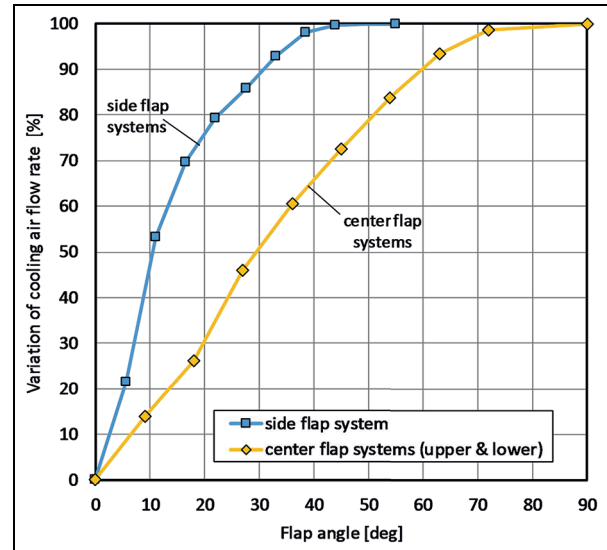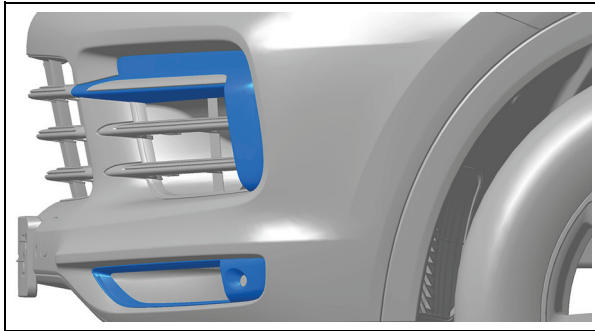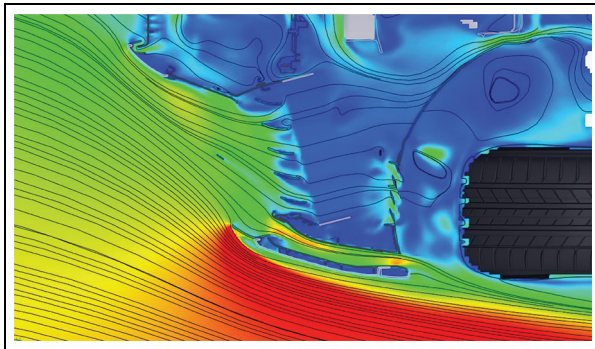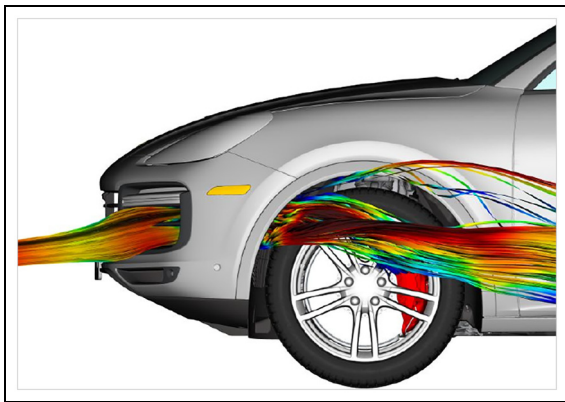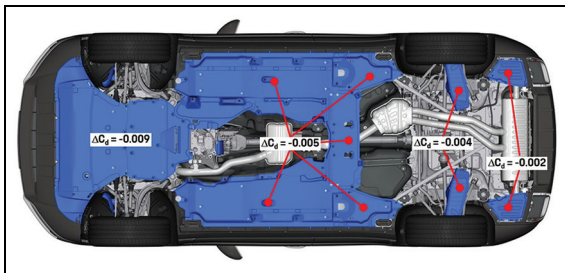
Figure 14. Air blades on the Cayenne – side view.

Figure 15. Air curtain througflow, z-section, plan view.

Figure 16. Air curtain and airflow around wheel, side view.

Figure 17. View of underbody panels.

the air throughput through the charge air coolers by 4% while also reducing drag through optimisation of the airflow around the sides of the front end. Air blades

are always advantageous when the outer edges of the side air inlets are located far to the outside and are therefore already situated within the low-pressure area of the airflow around the front end. Without air blades, some of the cooling air would be sucked out of the air inlet again, disturbing the airflow around the sides of the front end.

Air curtains

A further measure for reducing drag are the air curtains located in the sides of the front end, the air inlets of which are integrated in the cooling air inlets for the charge air coolers (see Figure 11). Depending on the engine version and wheel sets, the air curtains on the current Cayenne reduce the drag by three drag counts on average. Figures 15 and 16 show the air curtain throughflow from a CFD simulation.

Underbody

The underbody configuration of the Cayenne is based on the PL73 platform developed by Audi. From the outset, this platform represented an outstanding base for further detail optimisations and adaptations (Figure 17). The braking air ducts were integrated in the side underbody panels in the front end area. Further adaptations were made in the areas of the wheel spoilers and in the rear end area depending on the various engine versions. On some engine versions, a ventilation measure was integrated in the area of the hang-on transmission. The underbody panellings shown in Figure 17 reduce the drag by $\Delta C_d = -0.02$, that is, 20 drag counts.

Rear end

Design of the rear end and the rear airflow guidance has a significant influence on the base pressure, drag and rear-axle lift, particularly in the case of hatchback and squareback vehicles. One of the most important geometric parameters in this context is the inclination of the rear window, which is characterised by the so-called backlight angle. The influence of the backlight angle on drag and lift forces is the subject of numerous investigations,[36–42] most of which were carried out on simple bodies with small rear-end radii. The results have found their way into textbooks[31,43] and are frequently used in the automotive industry as design criteria for optimising and evaluating proportional models.

The main result from the studies mentioned above is that there is a significant change in the flow behaviour if a critical backlight angle is exceeded. This change represents the transition from hatchback flow to squareback flow. The critical angle depends strongly on the basic shape and edge radii at the rear end and lies in a range of 30°–38°,[38] compare Figure 19. From an angle of approximately 10°, drag increases progressively up to the critical angle. After exceeding the critical angle,
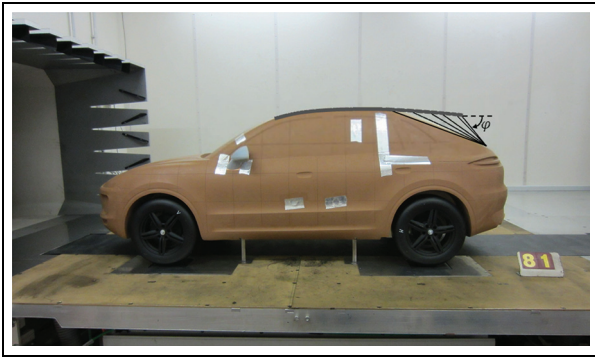
Figure 18. 1:3 Design-model used for parameter study of backlight angle.
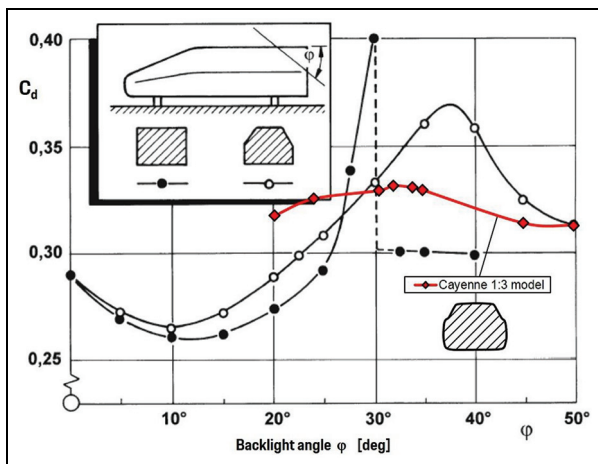
Figure 19. Variation of C_d with the backlight angle for the Cayenne 1:3 model in comparison to the data by Howell.[38] Figure taken from the textbook of Hucho.[44]

the drag generally decreases as the rear backlight angle continues to increase. The transition from hatchback to squareback flow can be associated with strong gradients in the drag and lift forces, which can lead to unsteady lift behaviour. For a real vehicle, this would be disadvantageous in terms of driving dynamics. In addition, a pronounced drag maximum occurs in the critical angular range. In reality, therefore, an attempt is made to avoid the critical angular range.

At this point, the question arises to what extent the results obtained from simplified bodies are relevant for practice, that is, for real vehicle development. And if so, which measures can prevent a drag increase in the critical range or are generally suited to reduce drag.

In order to clarify this question, a parameter study on the influence of the rear end configuration on drag was carried out within the framework of the 1:3 model phase.[26] The backlight angle was varied starting from the initial state of 35°. In addition, the effect of a roof spoiler and a combination of roof and side spoilers (fascia) was investigated for each backlight angle. The 1:3 model used for this purpose represented a defined

design stage and was equipped with rear view mirrors, structured underbody and a rear diffuser. The investigations were carried out in the model wind tunnel with 5-belt ground simulation, Figure 18.

Figure 19 first shows a comparison of the test results without any spoiler with the data documented in the textbook by Hucho,[31,44] which are based on an investigation by Howell.[38] In Figure 19, the test results have been superimposed with the original graph at the reference point of 50°. As can be seen, the curve determined on the Cayenne model is significantly flatter than those provided in the literature. There is no clear peak in C_d and no 'critical' backlight angle. The cause behind these discrepancies lies with the models used. While in the work of Howell a generic model with slanting sides, straight roof and small edge radii was used, the Cayenne model is based on a real design state with a sloping roof, boat-tailing, and rounded D-pillars. The model was also equipped with a structured underbody and a rear diffuser. Furthermore, the results were determined on the Cayenne model with rotating wheels and a moving ground. To summarise, it must be noted that the dependency of the C_d value on the backlight angle on real vehicle models and design states can be significantly lower than indicated in the literature. This also means that the backlight angle alone is not necessarily a suitable aerodynamic design criterion for real vehicle configurations.

Figure 20 presents the results if a roof spoiler and a combination of the roof spoiler with side spoilers is added. Shown is the variation of drag ΔC_d versus the backlight angle in comparison to the base-line results without any spoiler. The roof spoiler had a flat shape and a length of 30 mm in line with the initial design state. At each backlight angle, it was installed as an extension of the sloping roofline, that is, the angle of the spoiler slightly varied for each backlight angle. The side spoilers were implemented from the base point of the rear window up to the rear edge of the roof spoiler.

From Figure 20, it can be seen that a roof spoiler is an appropriate measure for reducing drag of vehicles with large backlight angles. In the present case, the roof spoiler reduces drag in the case of backlight angles exceeding 37°, while it increases drag in the case of smaller backlight angles. The addition of side spoilers leads to a further and significant reduction in drag within a large angular range. It is clear that other spoiler angles (e.g. a steeply inclined spoiler) will lead to different results. However, the results of the study clearly demonstrate the great potential of a combination of a roof spoiler and side/D-pillar spoilers for reducing drag of hatchback and squareback vehicles and were fully confirmed on the full-scale development model of the Cayenne.

Therefore, all models of the new Cayenne are equipped with a combination of a roof and side spoilers. With the exception of the V8 Turbo, all the basic models of the Cayenne are equipped with a fixed roof spoiler, which generates the desired downforce at the
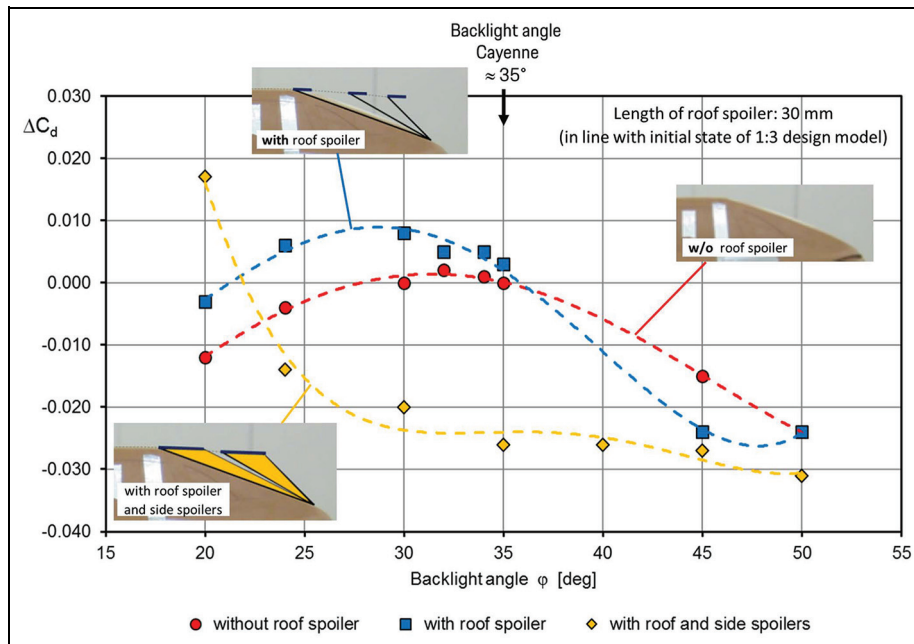
Figure 20. Influence of the backlight angle and the roof spoiler configuration on drag variation ΔC_d.
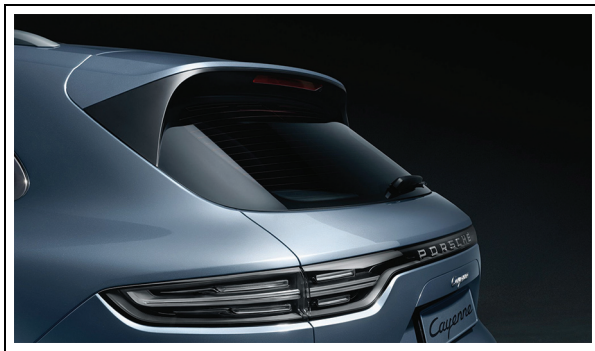
Figure 21. D-pillar spoilers (winglets) on the Cayenne S.

rear axle through a slight lip at the rear edge ('kicker'). Figure 21 shows the roof spoiler and the side spoilers (winglets) of the basic models. The side D-pillar spoilers[45] reduce the drag by $\Delta C_d = -0.007$.

Aero-wheel/brake cooling

A further measure for reducing drag was the development of an aerodynamically optimised 19" wheel for the basic Cayenne version. The development of such aerodynamically optimised wheels has recently gained increasing importance,[7,46] since the wheels account for up to 25% of the vehicle drag[47] and thus offers great optimisation potential. In recent years, considerable efforts have therefore been made to investigate the aerodynamics of rotating wheels and to develop measures to reduce the aerodynamic drag of wheels. The work of Landström et al.[48] and Vdovin[49,50] and, more recently, two *Forschungsvereinigung Automobiltechnik e.V., Germany* (FAT) research projects,[51,52] which

aimed to develop measures to reduce the drag of tyres on the one hand and to reduce the ventilation drag of rims on the other, should be highlighted here.

The aerodynamic drag of a rotating wheel is composed of the longitudinal drag and the so-called ventilation drag, which results from the rotation of the wheels and is caused by surface friction and uneven pressure distribution at the spokes.[53] The ventilation drag of the wheels can count up to 8% of the drag of a vehicle.[46] Recent findings show that the ventilation drag of a wheel is distributed approximately evenly over 50% of the tyres and 50% of the rims.[52] The aim of developing an aerodynamically optimised wheel must therefore be to minimise the aerodynamic drag and the ventilation drag. In the case of the Cayenne, however, no influence could be exerted on the tyre development and selection, so that the development focused on the realisation of an aerodynamically optimised rim.

At this point, it should not be forgotten that, in addition to aerodynamic aspects, other aspects play a major role in rim development in reality, Figure 22. Apart from the design, in a sporty SUV these are above all sufficient brake cooling as well as weight and costs. The development of an aerodynamically optimised rim therefore represents a considerable challenge in the field of tension between these requirements.

For the Cayenne, the target was a reduction of 0.005 in C_d in relation to a defined reference variant on the predecessor vehicle. In the design phase, the rim was primarily developed in the wind tunnel and in the evaluation and selection phase, supported by CFD, which was also used for evaluation of brake cooling. The method used to predict brake cooling, that is, the heat transfer coefficients and cool down times at the brake discs is based on a work by Schütz.[54] The use of CFD
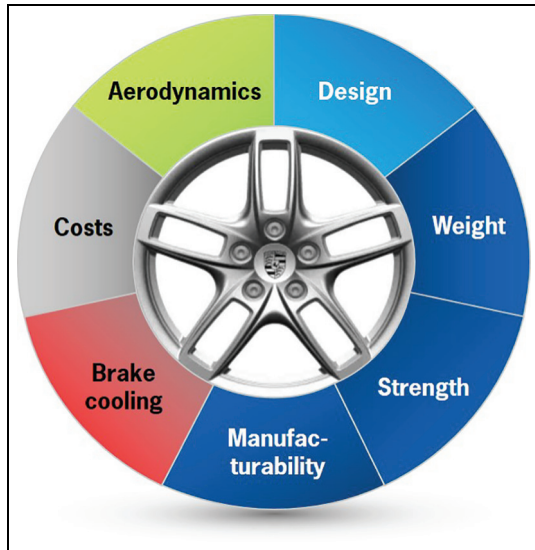
Figure 22. Criteria for rim development.

has the advantage that it provides the ventilation drag and its distribution on tyres and rims as a waste product, that is, without much additional effort.[46] On the other hand, however, there are very high computing times and costs. In wind tunnels, on the other hand, many variants can be evaluated aerodynamically in a relatively short time, but the ventilation drag cannot easily be determined[46]; a reliable measurement procedure was only recently developed within the framework of the FAT project.[52,53]

A reduction of the rim throughflow has proven to be effective for aerodynamic rim optimisation in all previous research work.[48–52] In addition to design of the

spokes, the free rim cross-section is therefore the most significant variable for reducing drag at the rim. For this reason, wheel versions featuring different rim covers were investigated in 2014 during preliminary tests in the S2A wind tunnel. Subsequently, the influence on brake cooling and on the heat transfer coefficients at the brake disc was evaluated for the most promising versions based on CFD simulations. Figure 23 shows the results of the preliminary trials; the various versions are classified from left to right according to increasing C_d advantage. The ventilation drag is not taken into account in this illustration because it could not be determined at the time of the wind tunnel campaign.

However, the results of the afore mentioned FAT project[52] allow conclusions to be drawn about the ventilation drag of the variants shown in Figure 23 because very similar covering measures were examined there on the basis of a similar 18" reference rim. Since the changes between the investigated covering variants were only very small and the ventilation drag decreases with increasing covering degree of the rim up to the full closure, it can be concluded from these results that the consideration of ventilation drag would not cause a change of the variant sequence in Figure 23.

As expected, Figure 23 shows a rough correlation with the throughflow cross-section of the rim. The advantage in terms of drag increases as the cross-section is reduced. Based on this illustration, it was determined that the free cross-section of the Aero-rim must not exceed 5 dm^2 in order to achieve a C_d improvement of 0.005 compared to the reference rim, which is shown in the centre of Figure 22.

One of the best variants in terms of drag is the 'outer ring' cover version, in accordance with the results of
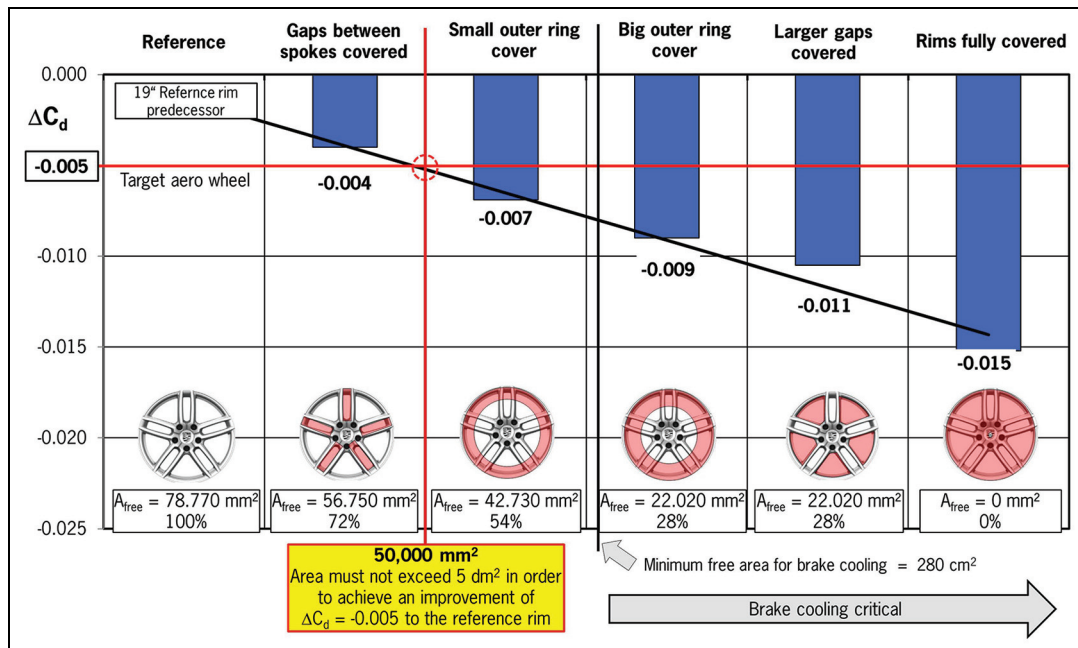

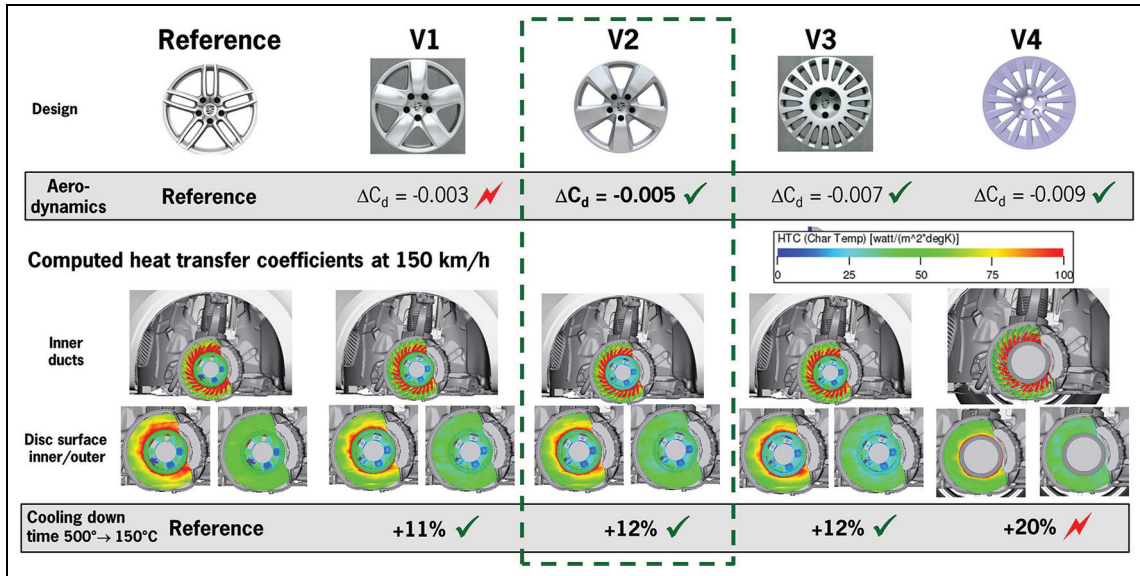**Figure 23.** Rim covers – C_d versus rim cross section.

Figure 24. Influence on brake cooling.

Landström[48] and the FAT project of 2016.[52] This variant, however, also has the greatest negative influence on brake cooling (see Figure 24) and was also rejected by the design department. With regard to brake cooling, a maximum worsening of the heat transfer coefficients and of the cooling-down times of about 10% with respect to the reference rim was accepted. A boundary design condition here was the load case slow downhill driving with trailer load. In Figure 23, the minimum cross-section of $280 \, cm^2$ is also entered, which was generally applied based on past experience gathered during sports car development to ensure brake cooling during rim development. As can be seen, this stipulation also fits in well with the requirements relating to brake cooling in the present case. During the further course of development, a series of rim

designs was evaluated aerodynamically[11] and in terms of brake cooling, whereby the ventilation drag was also taken into account with the aid of CFD. Figure 24 shows the variants that were shortlisted.

Aerodynamically advantageous and in accordance with the results of the FAT report no. 291 was the variant 'V2' with significantly widened spokes. This variant has approximately 50% lower ventilation drag than the reference rim.

Ultimately, the rim version shown in Figure 25 with a throughflow cross-section of $5.1 \, dm^2$ was selected because only this met all the requirements. During driving tests on the Grossglockner alpine road, this version was also confirmed to meet the brake cooling requirements.

Adaptive roof spoiler of the Cayenne Turbo

With a power of 550 hp, the V8 Turbo is the performance version of the current Cayenne. It differs from the basic version through the 2-inch larger 21" wheels and significantly wider tyres (front tyres + 30 mm, rear tyres + 40 mm) and a more striking front-end design. The objective was to compensate these aerodynamically negative effects through additional measures.

Around half of the C_d disadvantage compared to the basic version is compensated by the air suspension installed as standard on the Turbo, which lowers the vehicle from its initial reference position by 28 mm at 130 km/h and by a further 10 mm from 210 km/h. The effect of the ride height reduction on rear lift and on drag can be depicted from the ride height maps shown in Figures 26 and 27. From Figure 26, it can be seen that a parallel ride height reduction at the front and rear axle has no significant effect on rear lift. Figure 27 shows the effect on drag. As can be seen, the lowering of the ride height by 28 mm leads to a reduction of C_d by about –0.008. However, since the road position of

Figure 25. Final aero rim of the Cayenne, see also Figure 6.
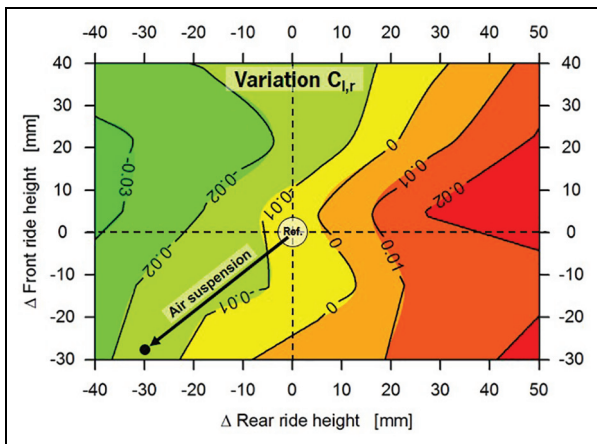
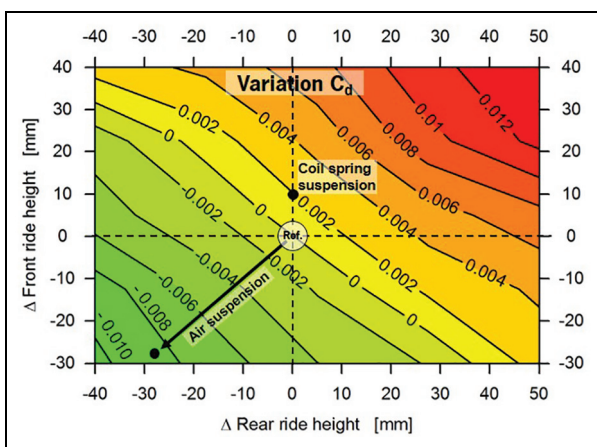**Figure 26.** Ride height map rear lift $C_{l,r}$ – Cayenne Turbo.

Figure 27. Ride height map C_d – air versus coil spring suspension.

Figure 28. Adaptive roof spoiler of the Turbo.

the coil spring suspension on the basic Cayenne versions is 10 mm higher at the front axle than the reference position of the Turbo, the overall drag benefit of the Turbo compared to the basic versions is of about $\Delta C_d = -0.010$, Figure 27. The remaining disadvantage is compensated by means of an optimised roofline and in conjunction with a deployable roof spoiler,[55] Figure 28.

The C_d reduction at the roofline results from an extension of the roof spoiler by 46 mm in conjunction with a lowering of the spoiler rear edge by 17 mm (in comparison with the fixed roof spoiler of the Basic Cayenne in both cases; Figure 29). Because lowering of the spoiler rear edge on the V8T results in a loss of downforce at the rear axle in comparison with the Basic Cayenne, use of a deployable roof spoiler was planned from the outset for the V8T in order to achieve the desired driving dynamics target value $C_{l,r} = -0.03$ at high speeds through an active spoiler element.

Pre-development of the deployable roof spoiler was already complete at the start of the project and, with a maximum spoiler deployment height of 80 mm and various intermediate positions, provided additional opportunities to positively influence the aerodynamics on the Turbo. Figure 30 shows the individual spoiler settings and functions. The aerodynamic spoiler polar is shown in Figure 31.

The deployable spoiler can move to a total of five positions. The lowest drag is achieved in the first, retracted position, the so-called 'ECO position'. In the second position, the 'Performance position', in which the spoiler is deployed to a height of 20 mm, the rear axle lift target value of $C_{l,r} = -0.03$ is achieved. This position is moved to automatically at a speed of 160 km/h. In the third position, the so-called 'Sport Plus' position, the spoiler is deployed to a height of 40 mm to generate even greater downforce at the rear axle ($C_{l,r} = -0.05$). This position is moved to when the Sport Plus button is actuated manually and is intended for sporty or race-track driving. The fourth position is the so-called 'compensation position' with a deployment height of 60 mm. This position is moved to automatically when the panoramic roof is open. The reason for this is that an air deflector is deployed when the roof is open in order to prevent buffeting in the passenger compartment. Deployed to a height of 78 mm, the air deflector deflects the airflow away from the body, reducing the effectiveness of the roof spoiler. This results in a loss of downforce at the rear axle, which is compensated through the greater deployment height of the roof spoiler in the fourth position.

The fifth position, with the maximum deployment height of 80 mm is the so-called 'airbrake' position. This position is moved to in less than 1 s within a defined speed range during emergency braking. In the airbrake position, maximum downforce at the rear axle and simultaneously the maximum drag is achieved, see Figure 31. At a vehicle speed of 250 km/h the additional load generated at the rear axle is 78 kg. The braking distance during full braking is reduced by up to 2 m.

The roof spoiler control strategy depends on numerous boundary conditions and is adapted to the position of the cooling air flaps in the front end.[56] Figure 32 shows an overview of the roof spoiler control strategy for the current V8 T.
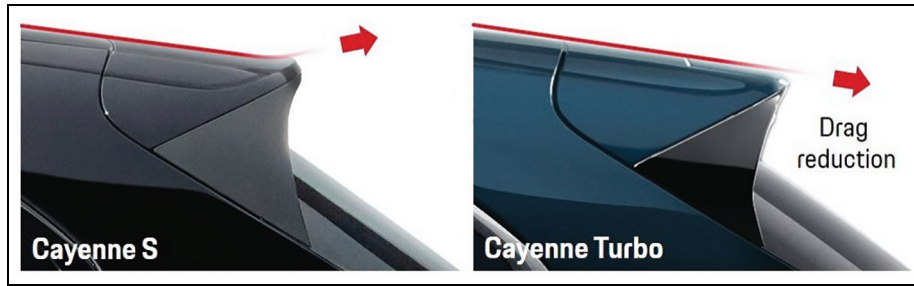
Figure 29. Turbo roofline compared to the 'S'-model.
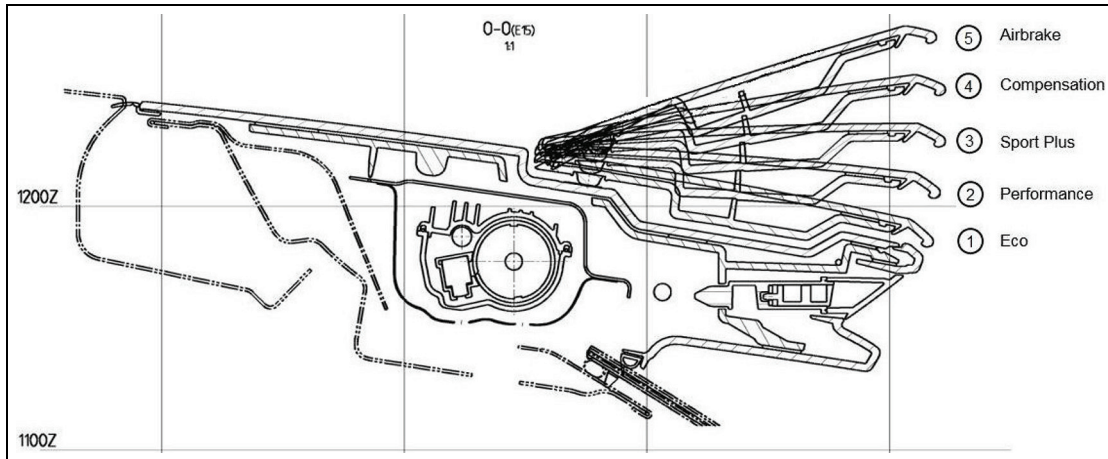

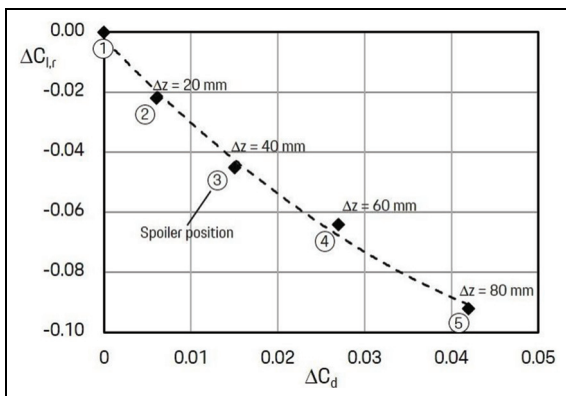**Figure 30.** Overview of spoiler positions.

Figure 31. Aerodynamic roof spoiler polar.

Figure 33 shows the rear axle lift/downforce characteristic against vehicle speed. The target rear axle lift is $C_{l,r} = -0.03$ and should be achieved from a vehicle speed of 160 km/h. Because the cooling air flaps open from approximately 200 km/h as the vehicle speed increases, the rear axle lift coefficient is slightly better than the target value in this speed range.

A major focus was placed on functional reliability during the development of the active aerodynamics and of the deployable roof spoiler. It had to be ensured that the customer is able to drive the vehicle safely and with a high degree of driving stability at all times, even in the event of a malfunction such as failure of one of the active systems.

Soiling/exterior water management

Soiling prevention of side glasses and exterior mirrors are safety- and comfort-relevant topics, which are closely linked to the aerodynamic flow and therefore represent a fundamental task of aerodynamic development. The work of Gaylard et al.[57] gives an excellent overview of the history of this topic and the current status regarding procedures and development tools.

Comfort and soiling prevention measures for the front side glasses and door mirrors glasses already played an important role in the first generation of the Cayenne. On the current Cayenne, a further improvement was achieved. This was realised through an optimised water drainage system at the A-pillar in conjunction with the hydrophobic coating on the side windows already used on the predecessor model. The hydrophobic coating has the advantage that even during heavy rainfall, the view to the mirrors through the side windows is barely impaired because the larger water streams are broken up into numerous small water and droplet streams. The advantages of a hydrophobic coating of the side glasses were already investigated and proven in a pre-development project in 1998.[58] The hydrophobic coating was first introduced
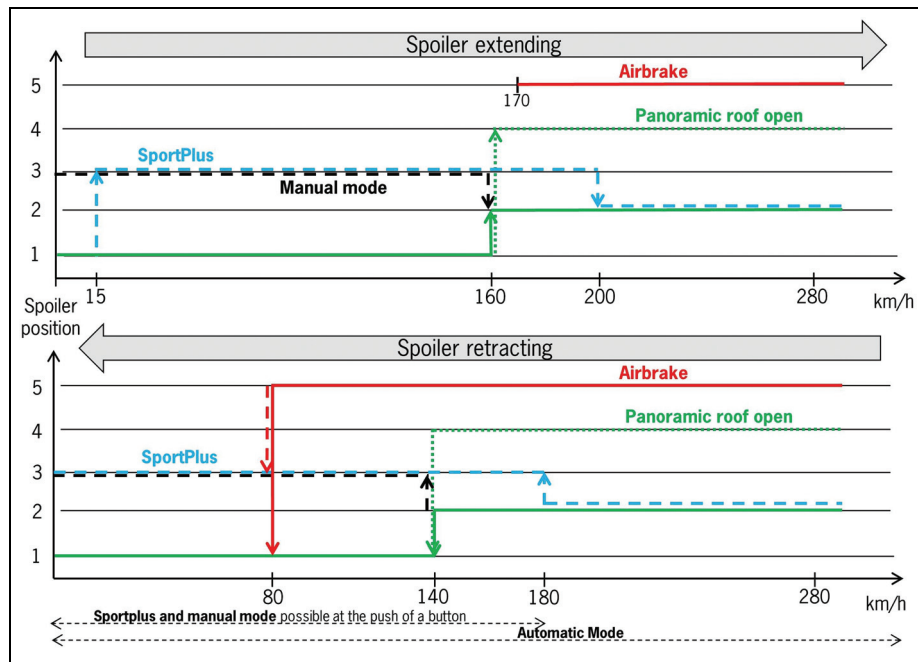
Figure 32. Control strategy for the adaptive roof spoiler on the current Cayenne Turbo.
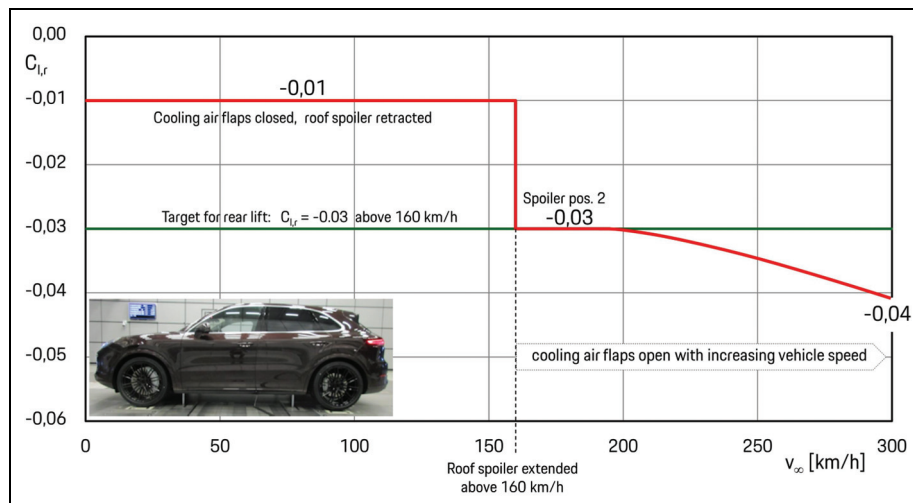

Figure 33. Rear-axle lift coefficient $C_{l,r}$ of the Turbo against vehicle speed.

on the 911 from model year 2004 and has since been used in almost all model lines.
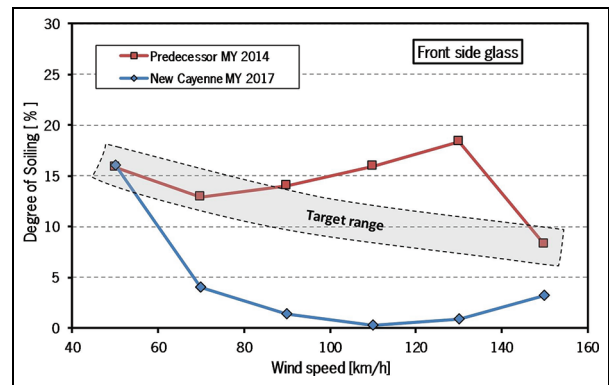
The patented water management system for the door mirrors[59] was originally developed for the 911 sports car and consists of a rain gutter at the top of the housing and a dripping edge on the underside, whereby the droplet channel and dripping edge overlap at the outside of the mirror housing, Figure 34. This system is now well proven and is today used on nearly all model lines.

In recent years, computational fluid dynamics has become increasingly important for assessing vehicle soiling.[57,60,61] Therefore, at the beginning of the project an internal study[62] was carried out to investigate the suitability of CFD for the simulation of vehicle soiling

and to compare it with experimental results. The numerical simulations were carried out with PowerFLOW, whereby not only the test vehicle but also the experimental test setup was mapped in detail. The results of the study showed a very good agreement of the simulation results with the experimental results for the side glasses and the vehicle body even at the rear. This is in agreement with the results of other authors.[7,57] However, the results for mirror glass contamination on the door mirror were not satisfactory. Here, it was shown that the effect of rain gutters and dripping edges could not be satisfactorily reproduced by the flow simulations. These, however, are the main measures for reducing mirror glass contamination. In addition, the use of CFD is currently still associated
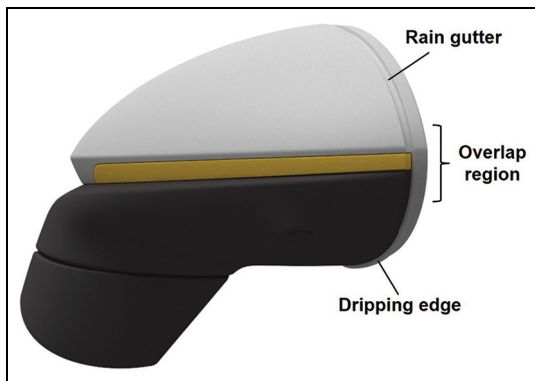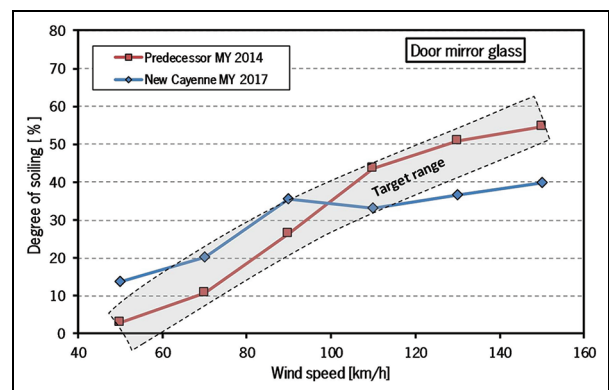
Figure 34. Door mirror of the current Cayenne and measures for soiling reduction,[59] side view.
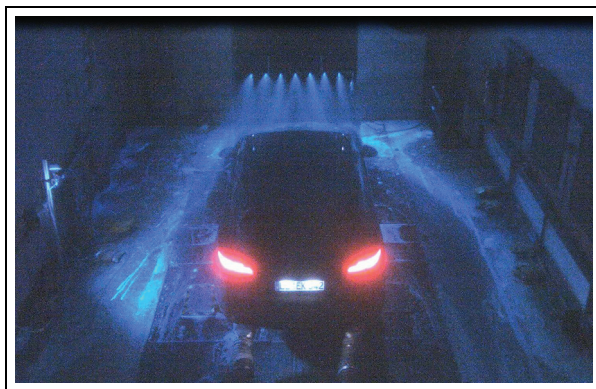

Figure 35. Soiling test setup in the FKFS thermal wind tunnel.

Figure 36. Soiling test with fluorescent water under UV illumination (rear top view).

Figure 37. Degree of soiling versus vehicle speed, front side glass.

Figure 38. Degree of soiling versus vehicle speed, mirror glass.

with considerable computational effort and costs, which are far higher than those of the experimental approach. For this reason, soiling optimisation on the Cayenne was carried out exclusively experimentally.

Since 2006, development and experimental testing of the soiling prevention measures have been conducted at the FKFS thermal wind tunnel using fluorescent water, Figures 35 and 36. In addition to subjective assessments, the FKFS's video, image processing and evaluation system DiVeAn[25] enables an objective evaluation in the form of key performance indicators such as degree and intensity of soiling. For the tests, a duration of 2 min per test run and a water volume of 400 L/h (roughly representative of heavy rainfall) have proven expedient. A reference mirror or a reference/predecessor vehicle are used as a control. In addition, benchmark measurements are carried out on competitor vehicles and used for comparison purposes. It should be noted at this point that vehicle soiling is often perceived very subjectively by test persons. In addition to the evaluation by objective indicators, a subjective assessment of the soiling tendency in the context of test drives and road trips is therefore indispensable.

Figures 37 and 38 show the evaluation of the validation measurements on the new Cayenne against the vehicle speed for the front side glass and the door mirror glass compared to the predecessor vehicle. The degree of soiling versus vehicle speed in comparison to the predecessor is shown. The degree of soiling represents the percentage of the soiled area related to the whole area of the region of interest. Details of the method applied can be found in the work of Spruss et al.[25]

The results shown in Figures 37 and 38 are typical for side glass and mirror glass soiling. As the speed increases, the degree of soiling of the side glass
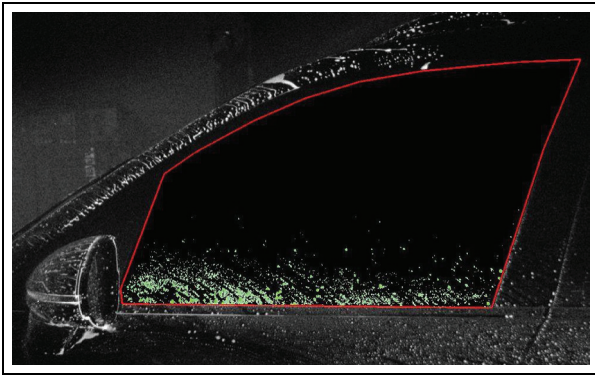
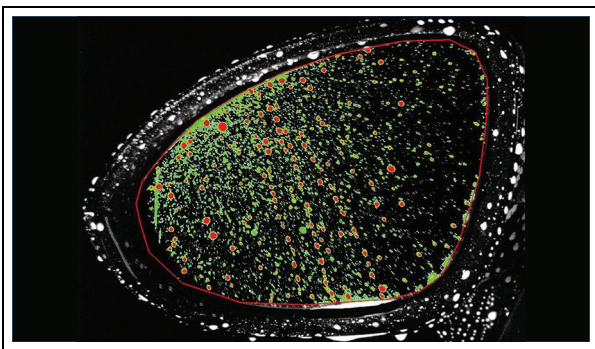**Figure 39.** Side glass at 70 km/h (DiVeAn).

Figure 40. Mirror glass at 70 km/h (DiVeAn).

decreases while it increases for the mirror glass. The reason for the former is that the A-pillar vortex becomes stronger with increasing speed and therefore pulls the water away from the side glass upwards over the roof. The degree of soiling of the mirror glass depends primarily on the amount of water hitting the mirror housing and the vorticity in the wake of the door mirror. Since both increase with increasing speed, the degree of contamination of the mirror glass generally increases with increasing speed. This also explains why at higher speeds the degree of soiling of the door mirror glasses is usually higher than for the side glasses. Of course, these conditions ultimately depend on the measures implemented to reduce soiling. However, it clearly shows that the real challenge lies in reducing mirror glass contamination.

Figures 39 and 40 show a visual representation of the side glass and mirror glass contamination at 70 km/h generated with the FKFS software DiVeAn. This type of visualisation is very helpful for assessing vehicle soiling during the development of measures. However, they require a certain experience in handling, since even smallest droplets are detected, for example, caused by condensation during the test, which may not be relevant in reality.

As can be seen from Figure 39, the side windows remain virtually free of soiling, that is, the water management at the A-pillar in conjunction with the

Table 4. Aerodynamics of the new Cayenne.

Cayenne model	Base	S	Turbo
Drag coefficient C_d	0.34	0.34	0.34[a]
Front lift coefficient $C_{l,f}$	0.17	0.17	0.17
Rear lift coefficient $C_{l,r}$	−0.03	−0.03	−0.03
Frontal area A	2.83 m^2	2.83 m^2	2.82 m^2
Drag area C_dA	0.962 m^2	0.962 m^2	0.987 m^2

[a]Official technical data for the Turbo is $C_d = 0.35$.

hydrophobic coating functions perfectly. In the visualisation of mirror glass contamination (Figure 40), only the larger (red) drops are relevant for reality. Overall, mirror glass contamination can be regarded as satisfactory, which was confirmed on extensive test drives in hot and cold countries in direct comparison with the predecessor vehicle and in comparison with competing vehicles.

The soiling optimisation on the Cayenne also shows that measures to reduce soiling, if carefully optimised, do not necessarily have to have significant adverse effects on the drag coefficient.[63,64] The rain gutters on the A-pillars are neutral with respect to drag and the two exterior mirrors increase the drag coefficient only by $\Delta C_d = +0.001$ (frontal area corrected). However, since the two exterior mirrors cause an increase in frontal area of approx. 0.06 m^2, the drag area C_dA increases by 2.4%.

Aerodynamics of the new Cayenne

Table 4 provides a summary of the aerodynamic data for the new Cayenne with the current engine versions. It should be noted that the C_d values are specified for closed radiator shutters and on the V8 Turbo for closed radiator shutters and retracted roof spoiler, while the lift coefficients apply for fully opened shutters as these are values relevant to driving dynamics at high vehicle speeds. It should also be noted that at $C_d = 0.34$, the standard Cayenne Turbo achieves a lower C_d value than the one indicated in the official technical data.

The Figures 41 and 42 show the variation of the drag coefficient C_d and the rear lift coefficient $C_{l,r}$ versus the angle of yaw at 140 km/h. The characteristics also show an improvement compared to the predecessor vehicle in the relevant range of ±5° yaw angle.

Figures 43 and 44 finally show the C_d values for the new Cayenne in a historical context. Depending on the engine version, the C_d value is reduced by 10–30 drag counts or 3–8% from generation to generation. Figure 44 shows this development in detail for the Cayenne S, taking into account the various facelifts. In relation to the first generation of the Cayenne, the C_d value was reduced by 0.05 or 13% by the current generation. Simultaneously, the vehicle cross-section has increased from 2.79 to 2.83 m^2, so that the improvement in the drag area C_dA is slightly smaller at 11.5%.
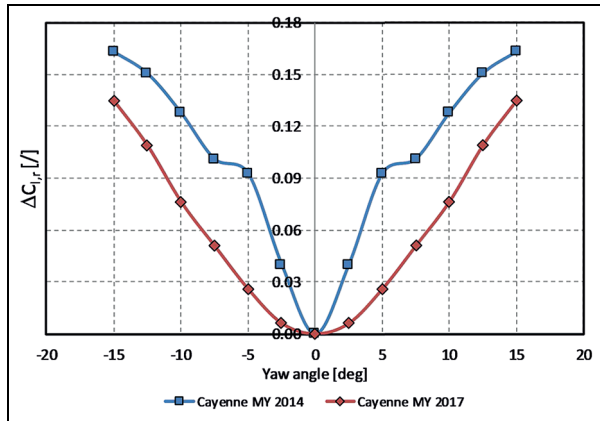
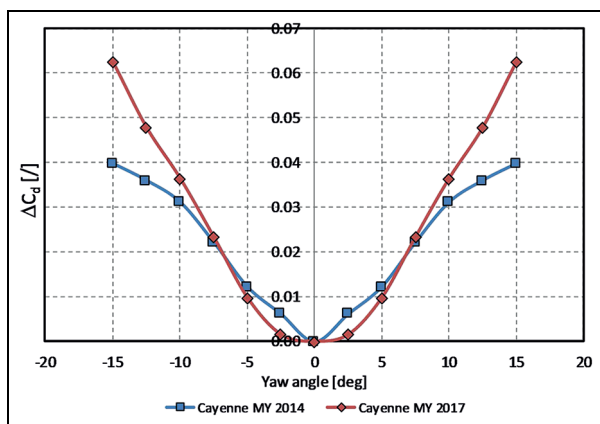**Figure 41.** Drag coefficient C_d versus yaw angle.

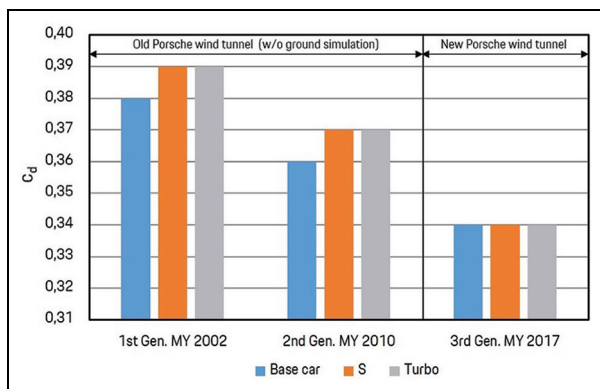**Figure 42.** Rear lift coefficient $C_{l,r}$ versus yaw angle.

Figure 43. Development of C_d value since 2002.

Conclusion

An overview of the aerodynamic development and the aerodynamic properties of the new Porsche Cayenne has been given. Based on a brief description of the development process, the development objectives and the tools used, the individual aerodynamic optimisations have been described. In addition to the detailed aerodynamic optimisation, the key to reducing drag lay in the reduction of the cooling air losses through an
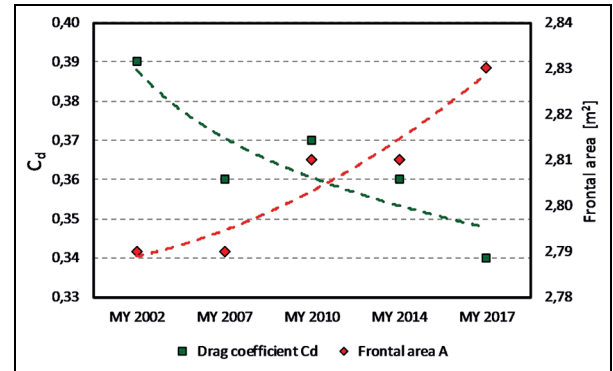

Figure 44. C_d value/frontal area, Cayenne S.

active and demand-based control of the cooling air mass flows. The implemented air flap system enables complete closure of all air inlet openings and reduces drag by 6%. On the new Cayenne Turbo, an adaptive roof spoiler has been added as an active element, which reduces drag in the retracted position and ensures the necessary rear axle downforce for optimum driving dynamics in the various deployed positions.

On average, the new Cayenne achieves a drag coefficient of $C_d = 0.34$. Compared to the predecessor vehicle, the drag has thus been reduced by 5%. The adaptive aerodynamics concept of the new Cayenne contributes significantly to this and enables a maximum spread between Eco and Performance, that is, the optimal compromise between fuel consumption, performance and comfort, under all driving conditions.

ORCID iD

Thomas Wolf ![iD] https://orcid.org/0000-0002-7262-8353

References

1. *Global technical regulation on Worldwide harmonized Light vehicles Test Procedures (WLTP)*. ECE/TRANS/ 132, Addendum 15: Global technical regulation No. 15 (GTR15). Geneva: United Nations Economic Commission for Europe, 2017.
2. Kotapati R, Keating A, Kandasamy S, et al. The Lattice-Boltzmann-VLES method for automotive fluid dynamics simulation, a review. SAE paper 2009-26-057, 2009.
3. Chen H, Teixeira C and Molvig K. Digital physics approach to computational fluid dynamics: some basic

theoretical features. *Int J Mod Phys C: Comput Phys Phys Comput* 1997; 8: 675–684.

4. Chen S and Doolen GD. Lattice Boltzmann method for fluid flows. *Ann Rev Fluid Mech* 1998; 30: 329–364.

5. Palin R, Johnston V, Johnson S, et al. The aerodynamic development of the Tesla model S – part 1: overview. SAE paper 2012-01-0177, 2012.

6. Kandasamy S, Duncan B, Gau H, et al. Aerodynamic performance assessment of BMW validation models using computational fluid dynamics. SAE paper 2012-01-0297, 2012.

7. Chaligné S, Turner R and Gaylard A. The aerodynamics development of the new land rover discovery. In: *Progress in vehicle aerodynamics and thermal management. Proceedings of the 11th FKFS-conference*, Stuttgart, 26–27 September 2017. Cham: Springer.

8. Iinuma Y, Taniguchi K and Oshima M. Aerodynamics development for a new EV hatchback considering crosswind sensitivity. SAE paper 2018-01-0715, 2018.

9. Stumpf H, Röser P, Wiegand T, et al. The new aerodynamic and aeroacoustic wind tunnel of the Porsche AG. In: *15th Stuttgart international symposium*, FKFS, Stuttgart, 17–18 March 2015.

10. Cogotti F, Pfadenhauer M and Wiegand T. Potential of Porsche reference cars for aerodynamic development. In: *Proceedings of the 11th FKFS-conference*, Stuttgart, 26–27 September 2017. Cham: Springer.

11. Wolf T. Die Aerodynamikentwicklung des neuen Porsche Cayenne. In: *13th conference on vehicle aerodynamics*, Munich, July 3–4, 2018. Essen: Haus der Technik e.V.

12. Vagt JD and Wolff B. The new aerodynamic test center – two new wind tunnels at Porsche – part 1&2. *Automobiltechnische Zeitschrift (ATZ)* 1987; 89: 121–129;183–189.

13. Berndtsson A, Eckert WT and Merker E. The effect of groundplane boundary layer testing in a wind tunnel. SAE paper 880248, 1988.

14. Eckert W, Singer N and Vagt JD. The Porsche wind tunnel floor-boundary-layer control – a comparison with road data and results from moving belt. SAE paper 920346, 1992.

15. Mueller R, Singer N and Eckert W. Moving belt with distributed suction in the Porsche model wind tunnel. SAE paper 1999-01-0650, 1999.

16. Christoffersen L, Landström C and Walker T. A wind tunnel study correlating the aerodynamic effect of cooling flows for full and reduced scale models of a passenger car. SAE paper 2010-01-0759, 2010.

17. Meinert F, Johannessen K, Saito F, et al. A correlation study of wind tunnels for reduced-scale automotive aerodynamic development. SAE paper 2016-01-1598, 2016.

18. Wolf T. Minimising the cooling system drag for the New Porsche 911 Carrera (Bernoulli Aerodynamics International, Vol. 1, 2007). In: *5th MIRA international vehicle aerodynamics conference*, Warwick, 13–14 October 2004. Warwick: MIRA.

19. *Methods and devices for determining mass flows of gaseous media through heat exchangers.* Patent DE3916529A1, 1989.

20. Stoll A. *Study and optimisation of measurement accuracy during the determination of cooling air mass flows in automobile radiators.* Degree Thesis, TU Dresden, Dresden, 2006 (in German).

21. Kuenstner R, Potthoff J and Essers U. The aero-acoustic wind tunnel of Stuttgart University. SAE paper 950625, 1995.

22. Wiedemann J and Potthoff J. The new 5-belt road simulation system of the IVK wind tunnels – design and first results. SAE paper 2003-01-0429, 2003.

23. Wittmeier F, Michelbach A, Wiedemann J, et al. The new interchangeable three-belt system in the IVK full-scale wind tunnel of University of Stuttgart: design and first results. SAE paper 2016-01-1581, 2016.

24. Waudby-Smith P and Bender T. The GIE S2A full-scale aero-acoustic wind tunnel. SAE paper 2004-01-0808, 2004.

25. Spruss I, Landwehr T, Kuthada T, et al. Advanced investigation methods on side glass soiling. In: *Progress in vehicle aerodynamics and thermal management, proceedings of the 9th FKFS-conference*, 1–2 October 2013. Renningen, Germany: Expert-Verlag.

26. Stegmaier T. *Aerodynamic optimisation of squareback vehicles.* Degree Thesis, University of Stuttgart, Stuttgart, 2012 (in German).

27. Janssen LJ and Hucho WH. The effect of various parameters on the aerodynamic drag of passenger cars. In: Stephens HS (ed.) *Advances in road vehicle aerodynamics.* Bedford: BHRA Fluid Engineering, 1973.

28. Barnard RF. Theoretical and experimental investigation of the aerodynamic drag due to automotive cooling systems. *Proc IMechE Part D: J Automobile Engineering* 2000; 214: 919–927.

29. Kuthada T, Wittmeier F, Bock B, et al. The effects of cooling air on the flow field around a vehicle. SAE paper 2016-01-1603, 2016.

30. Baeder D, Indinger T, Adams N, et al. Aerodynamic investigation of vehicle cooling drag. SAE paper 2012-01-0170, 2012.

31. TC Schuetz (ed.). *Aerodynamics of road vehicles.* 5th ed. Warrendale, PA: SAE International, 2015.

32. Saab S, Hetet JF, Maiboom A, et al. Impact of underhood opening area on the drag coefficient and the thermal performance of a vehicle. SAE paper 2013-01-0869, 2013.

33. Saab S, Hetet JF, Maiboom A, et al. Combined modeling of thermal systems of an engine in the purpose of a reduction in the fuel consumption. SAE paper 2013-24-0142, 2013.

34. *Front of a motor vehicle.* US Patent 9694858, 2017.

35. *Luftleitvorrichtung für ein Kraftfahrzeug.* Patent DE102012111274A1, 2012.

36. Morel T. The effect of base slant on the flow pattern and drag of three-dimensional bodies with blunt ends. In: Sovran G, Morel T and Mason WT (eds) *Aerodynamic drag mechanisms of bluff bodies and road vehicles.* Berlin: Springer, 1978, pp.191–226.

37. Ahmed S, Ramm G and Faltin G. Some salient features of the time-averaged ground vehicle wake. SAE paper 840300, 1984.

38. Howell J. Shape and drag. In: W-H Hucho (ed.) *1st Euromotor short course 'using aerodynamics to improve the properties of cars'.* Stuttgart: University of Stuttgart, 1998.

39. Howell J and Le Good G. The effect of backlight aspect ratio on vortex and base drag for a simple car-like shape. SAE paper 2008-01-0737, 2008.

40. Fuller J and Passmore MA. The importance of rear pillar geometry on fastback wake structures. *J Wind Eng Indus Aerodyn* 2014; 125: 111–120.

41. Wood D. *The effect of rear geometry changes on the notchback flow field.* Doctoral Thesis, Loughborough University, Loughborough, 2015.

42. Rossitto R, Sicot C, Ferrand V, et al. Influence of afterbody rounding on the pressure distribution over a fastback vehicle. *Exp Fluids* 2016; 57: 43.

43. Barnard RH. *Road Vehicle Aerodynamic Design – An Introduction.* 3rd ed. St Albans: MechAero Publishing, 2009.

44. Schuetz T (ed.). *Hucho – Aerodynamik des Automobils.* 6th ed. Berlin: Springer-Verlag, 2013.

45. *Luftleiteinrichtung zur Anordnung im Heck- oder Dachbereich eines Kraftfahrzeuges.* Patent DE102007032322A1, 2007.

46. D'Hooge A, Palin R, Johnson S, et al. The aerodynamic development of the Tesla model S – part 2: wheel design optimization. SAE paper 2012-01-0178, 2012.

47. Wickern G, Zwicker K and Pfadenhauer M. Rotating wheels – their impact on wind tunnel test techniques and on vehicle drag results. SAE paper 970133, 1997.

48. Landström C, Walker T, Christoffersen L, et al. Influences of different front and rear wheel designs on aerodynamic drag of a sedan type passenger car. SAE paper 2011-01-0165, 2011.

49. Vdovin A. *Investigation of aerodynamic resistance of rotating wheels on passenger cars.* Engineering Thesis, Department of Applied Mechanics, Chalmers University of Technology, Gothenburg, 2013.

50. Vdovin A. Investigation of wheel ventilation-drag using a modular wheel design concept. SAE paper 2013-01-0953, 2013.

51. *Reifenentwicklung unter aerodynamischen Aspekten.* Bericht Nr. 252. Berlin: Forschungsvereinigung Automobiltechnik e.V. (FAT), 2013.

52. *Analyse, Messung und Optimierung des Ventilationswiderstandes von PKW-Rädern.* Bericht Nr. 291. Berlin: Forschungsvereinigung Automobiltechnik e.V. (FAT), 2016.

53. Link A, Widdecke N, Wittmeier F, et al. Measurement of the aerodynamic ventilation drag of passenger car wheels. *Automobiltechnische Zeitschrift* 2016; 118: 38–43.

54. Schütz TC. Coupled approach to brake cooling simulation. In: *7th MIRA international vehicle aerodynamics conference*, Birmingham, 22–23 October 2008.

55. *Rear air-guiding device.* US Patent 9567015, 2017.

56. *Method for setting a deployed position of a rear spoiler of a vehicle.* US Patent 2018/0050741, 2018.

57. Gaylard AP, Kirlan K and Lockerby DA. Surface contamination of cars: a review. *Proc IMechE Part D: J Automobile Engineering* 2017; 231: 1160–1176.

58. Chor D. *Grundsatzuntersuchung zur Seitenscheibenverschmutzung bei der aktuellen Porsche Fahrzeuggeneration und Definition geeigneter Abhilfemaßnahmen.* Diploma Thesis, University of Stuttgart, Stuttgart, 1998.

59. *Exterior rear view mirror for a motor vehicle.* US Patent 8727412, 2014.

60. Hagemeier T. *Experimental and numerical investigation of vehicle soiling processes.* Doctoral Thesis, University of Magdeburg, Magdeburg, 2012.

61. Allocco M. *Multiphase simulations for vehicle external water management.* Engineering Thesis, Politecnico di Torino, Torino, 2018.

62. Reifenrath M. *Numerische Simulation der Verschmutzung von Fahrzeugen.* Masters Thesis, University of Darmstadt, Darmstadt, 2016.

63. Bannister M. Drag and dirt deposition mechanisms of external rear view mirrors and techniques used for optimisation. SAE paper 2000-01-0486, 2000.

64. Olsson M. *Designing and optimizing side-view mirrors.* Master Thesis, Chalmers University of Technology, Göteborg, 2011.

Appendix I

Notation

A	frontal area (m^2)
A_{free}	projected through flow area of a rim (m^2)
A_i	net inlet area (m^2)
A_r	radiator face area (m^2)
C_d	drag coefficient
$C_{l,f}$	front lift coefficient
$C_{l,r}$	rear lift coefficient
dragcount	one drag count is equal to $\Delta C_d = 0.001$
α	flap rotation angle (°)
φ	backlight angle (°)
Δ	variation